JOURNAL OF GEOPHYSICAL RESEARCH, VOL. 114, B02309, doi:10.1029/2008JB005814, 2009

Structural features and shear-velocity structure of the "Pacific Anomaly"

Yumei He[1,2] and Lianxing Wen[1]

Received 19 May 2008; revised 27 October 2008; accepted 6 November 2008; published 18 February 2009.

[1] We constrain structural features and shear-velocity structure of a low-velocity anomaly in the lower mantle beneath the Pacific (we term it the "Pacific Anomaly") on the basis of forward travel time and waveform modeling of the observed direct *S*, *Sdiff*, *ScS*, *SKS*, and *SKKS* phases sampling a great arc across the anomaly from eastern Eurasia to southern South America. After correction for the effects of earthquake mislocation and the seismic heterogeneities outside the Pacific Anomaly, seismic observations suggest that the Pacific Anomaly along the great arc consists of at least two separated portions with a 740-km-wide gap between them. The western portion of the anomaly is about 1050 km wide, extends at least 740 km above the core-mantle boundary (CMB), and exhibits a trapezoidal shape with lateral dimensions increasing slightly with depth. The velocity structure of the western portion varies from −3.0% at the top (740 km above the CMB) to −3.5% at 100 km above the CMB and an average shear-velocity reduction of −5% in the bottom 100 km of the mantle. The eastern portion of the anomaly reaches at least 340 km above the CMB beneath the mid-Pacific with an 1800-km-wide base and has a uniform velocity reduction of −3%. Waveform modeling further suggests a very low velocity layer with a shear-velocity reduction of −10% located at the edge of the western portion of the anomaly. Combining the latest results from others, we present a general picture of structural and velocity structures of the Pacific Anomaly. The structural and velocity features suggest that the anomaly represents a cluster of metastable thermo-chemical piles.

Citation: He, Y., and L. Wen (2009), Structural features and shear-velocity structure of the "Pacific Anomaly," *J. Geophys. Res.*, *114*, B02309, doi:10.1029/2008JB005814.

1. Introduction

[2] Seismic tomography has revealed two broad, seismically slow anomalies in the lower mantle beneath the Pacific Ocean and Africa [e.g., *Dziewonski*, 1984; *Su et al.*, 1994; *Masters et al.*, 1996; *Li and Romanowicz*, 1996; *Ritsema et al.*, 1999; *Van der Hilst and Kárason*, 1999; *Ishii and Tromp*, 1999; *Gu et al.*, 2001; *Grand*, 2002; *Kustowski et al.*, 2008]. We name them the "Pacific Anomaly" and the "Africa Anomaly," respectively. Travel time analyses indicate that the African Anomaly reaches 1300 km above the core-mantle boundary (CMB) [e.g., *Ritsema et al.*, 1998; *Ni and Helmberger*, 2003; *Wang and Wen*, 2007]. Recent high-resolution waveform and travel-time analyses show that the African Anomaly exhibits an "L-shaped" base changing from a north-south orientation in the South Atlantic Ocean to an east-west orientation in the Indian Ocean [*Wang and Wen*, 2004] and a "bell-like" geometry in the middle-lower mantle along a great arc from the East Pacific Rise to the Japan Sea, with both the southwestern and the northeastern flanks tilting toward its center beneath southern Africa [*Wang and Wen*, 2007]. Detailed waveform modeling further revealed that the African Anomaly has steeply dipping edges and rapidly varying thicknesses [*Wen et al.*, 2001; *Wen*, 2001], with a strong negative shear velocity gradient from −2% (top) to −9 to −12% (bottom) in the lowermost 300 km of the anomaly [*Wen et al.*, 2001; *Wen*, 2001; *Wang and Wen*, 2004] and an average shear velocity reduction of −2 to −3% in the middle-lower mantle [*Wang and Wen*, 2007]. The geometric and velocity features of the anomaly indicate that the African Anomaly is compositionally distinct and geologically stable [*Wen et al.*, 2001; *Wen*, 2001, 2006; *Wang and Wen*, 2004, 2007].

[3] Seismic tomographic models showed that the Pacific Anomaly occupies a broad area at the base of the mantle (about 10,000 km across) and probably extends several hundred kilometers above the CMB. Some studies reported that the Pacific Anomaly has bulk sound velocity increase anticorrelated with shear velocity reduction [*Masters et al.*, 2000], a higher density [*Ishii and Tromp*, 1999] and sharp edges [e.g., *To et al.*, 2005; *Ford et al.*, 2006; *Takeuchi et al.*, 2008]. Waveform studies also revealed existence of ultralow-velocity zones (ULVZ) at the base of the mantle beneath western Pacific for both *P* and *S* waves [e.g., *Garnero and Helmberger*, 1996; *Wen and Helmberger*, 1998a, 1998b;

[1]Department of Geosciences, State University of New York at Stony Brook, Stony Brook, New York, USA.
[2]Key Laboratory of the Earth's Deep Interior, Institute of Geology and Geophysics, Chinese Academy of Sciences, Beijing, China.

0148-0227/09/2008JB005814$09.00

Vidale and Hedlin, 1998; *Rost and Revenaugh*, 2003] and some complex structures beneath the central Pacific [*Mori and Helmberger*, 1995; *Bréger and Romanowicz*, 1998; *Russell et al.*, 2001; *Wen*, 2002; *Avants et al.*, 2006; *Lay et al.*, 2006; *Ohta et al.*, 2008].

[4] The important unresolved issues related to the Pacific Anomaly are: the geographic extent of the anomaly; the nature of transition from the Pacific Anomaly to the surrounding mantle; whether the anomaly represents a massive low-velocity province like the African Anomaly or it consists of multiple portions; the depth extent and geometry of the anomaly in the lower mantle; the connection between the portion of the anomaly in the middle-lower mantle with its base; and the overall velocity structures of the anomaly in the lower mantle. As the high-resolution seismic studies of the African Anomaly have demonstrated, resolving these issues is crucial to our further understanding of the origin and dynamics of the Pacific Anomaly.

[5] With the deployment of many permanent and temporal seismic stations in Eurasia, the Pacific Ocean and South America, it becomes plausible to address some of these outstanding issues related to the Pacific Anomaly. In a recent study, we have mapped out some portion of the geographical boundary of the base of the Pacific Anomaly beneath the western Pacific Ocean and studied transitional structure from the Pacific Anomaly to the surrounding lowermost mantle along a cross section from Fiji to China [*He et al.*, 2006]. In this paper, we choose a great circle arc from eastern Eurasia to southern South America on the basis of event and station locations. We constrain structural features and shear velocity structure of the Pacific Anomaly throughout the mantle along the great arc using waveform modeling and travel-time analysis of direct *SH*, *Sdiff*, *ScS*, *SKS* and *SKKS* phases, and address other issues such as: whether the anomaly represents a massive low-velocity province or consists of multiple portions; the depth extent and geometry of the anomaly in the lower mantle; the connection between the portion of the anomaly in the middle-lower mantle with its base; and the overall velocity structures of the anomaly in the lower mantle. We present seismic data and our modeling procedures in section 2, discuss detailed constraints on the geometry and shear velocity structure in section 3, and discuss the implications of the seismic results in section 4.

2. Seismic Data and Method

2.1. Seismic Data

[6] The direct *S*, *Sdiff*, *ScS*, *SKS* and *SKKS* phases (Figure 1c) provide excellent constraints on the structural and velocity features of the Pacific Anomaly across the great arc. The absolute travel times of *S* and *SKS* phases can be used to place constraints on the thickness and the horizontal extent of the anomaly, respectively. Because *SKKS* and *SKS* phases have similar raypaths in both the source- and receiver-side upper mantle, the differential *SKKS-SKS* travel-time residuals are most sensitive to the velocity heterogeneities in the lower mantle and can be used to place constraints on the geometry and velocity structure of the Pacific Anomaly. The additional *ScS* travel-time residuals and waveforms provide further constraints on the geometry and velocity structure of the Pacific Anomaly.

[7] We collect broadband displacements of direct *S*, *Sdiff*, *ScS*, *SKS* and *SKKS* phases recorded at a distance range between 55° and 130° for all the events occurring in the Pacific Ocean from 1994 to 2008 with a magnitude greater than 5.8. We select seven events with simple source time functions and high signal-to-noise ratios. Because we analyze each phase and each event, we adopt a criterion of selecting a few events with the highest waveform quality without sacrificing the sampling coverage of the available data. These selected events occurred in the Solomon Islands, the Tonga-Fiji subduction zone, and the southern East Pacific Rise (see Figure 1b and Table 1), and encompass the sampling coverage of all the other events sampling the great circle arc. They are recorded in several permanent and temporary seismic networks. The permanent networks include the Global Seismographic Network (GSN), the Kazakh Network (KZ), the New China Digital Seismographic Network (NCDSN), the China National Digital Seismographic Network (CNDSN), the Chinese Capital Seismic Network (CCSN), the GEOFON, the GEOSCOPE and the F-net in Japan. The temporary arrays include the Northern China Interior Seismic Project (NCISP), the Southwest Pacific Seismic Experiment, the Micronesia Seismic Network, the Seismic Experiment in Patagonia and Antarctica and the Chile Argentina Experiment. Seismic data collected for these event-station pairs sample a great arc across the Pacific Anomaly from eastern Eurasia to southern South America within an azimuthal range of 18° (Figure 1b) and provide good sampling coverage in the lower mantle beneath the western Pacific (Figure 1a).

[8] All seismograms are deconvolved using their corresponding instrument responses, and are rotated to tangential, radial and vertical components. A butterworth filter with a frequency range of 0.008 – 1 Hz is applied to all seismograms.

2.2. Modeling Procedure

[9] Because the seismic data sample the Pacific Anomaly within a small azimuthal range of 18° (Figure 1b), we use simplified two-dimensional (2-D) models in our forward modeling. Our forward modeling consists of three procedures:

[10] 1. We re-determine location and origin time of the chosen earthquakes using seismic observations recorded by the GSN and a three-dimensional (3-D) shear velocity tomographic model (S. Grand, personal communication, 2004). Detailed relocation results are presented in the Appendix.

[11] 2. We correct for the travel-time residuals that are caused by the seismic heterogeneities outside the Pacific Anomaly. The corrections consist of travel-time residuals predicted on the basis of the shear velocity tomographic model and an additional component associated with the underestimation of the shear velocity tomographic model. The corrected travel-time residuals can be attributed to the Pacific Anomaly.

[12] 3. We obtain the best fitting model for the Pacific Anomaly through trial-and-error forward modeling of the corrected shear wave travel-time residuals. When the direct *S*, *Sdiff*, and *ScS* phases are involved, we apply the *SH* hybrid method [*Wen*, 2002] to calculate synthetic seismograms and travel-time residuals are obtained on the basis of

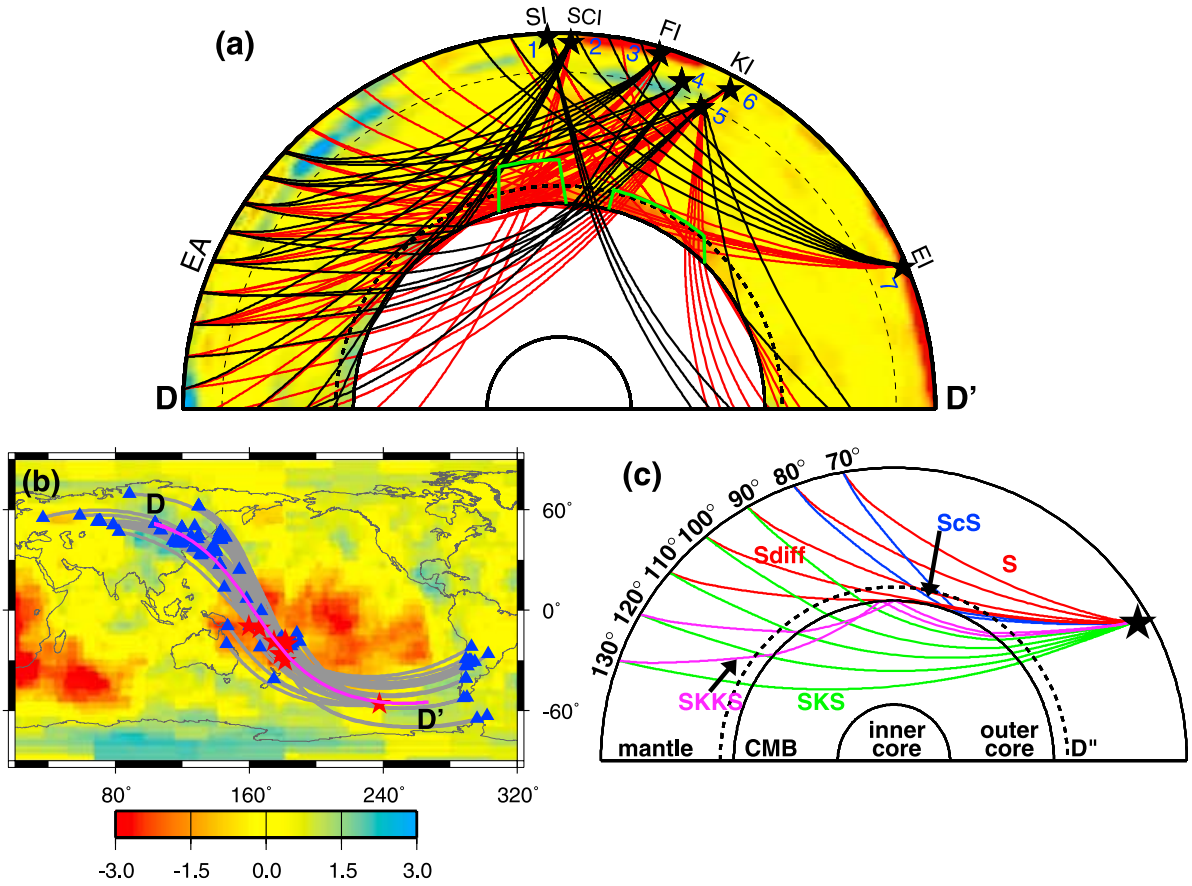

Figure 1. (a) Best fitting model (green contour) and raypaths of the seismic phases used to constrain the structural features and shear velocity structure of the Pacific Anomaly in a two dimensional cross section along Eurasia (EA) to southern South America. Black and red traces represent propagation paths without and with observed travel-time delays that can be attributed to the Pacific Anomaly, respectively. Seven selected events (from 1 to 7; see Table 1) occurred in the Solomon Islands (SI), the Santa Cruz Islands (SCI), the Fiji Islands (FI), the Kemadec Islands (KI), and the Easter Island (EI). The best fitting model of the western portion has a shear-velocity structure with velocity reductions gradually decreasing from −3.0% at 740 km above the CMB to −3.5% at the 100 km above the CMB, and an average shear-velocity reduction of −5% in the bottom 100 km of the mantle. The eastern portion has a uniform velocity structure of −3%. Black stars represent seismic events. The background is shear-velocity perturbations from a global shear-velocity tomographic model (S. Grand, personal communication, 2004). (b) Map view of great circle paths (gray traces), locations of earthquakes (red stars), and seismic stations (blue triangles). The purple curve represents the 2-D cross section illustrated in Figure 1a. (c) Raypaths of direct *S*, *Sdiff* (red lines), *ScS* at epicentral distances from 70° to 80° (blue lines), *SKS* at epicentral distances from 90° to 130° (green lines), and *SKKS* at epicentral distances from 120° to 130° (purple lines). These raypaths are calculated on the basis of PREM and a source depth of 300 km.

those synthetic seismograms. The hybrid method is a combination of the generalized ray theory, a finite difference technique and the Kirchhoff theory, so the finite frequency effect of wave propagation is taken into account in the forward calculations of travel time.

[13] The absolute travel times of direct *SH*, *SHdiff*, *ScS* and *SKS* phases are obtained by the cross-correlation method. We first choose one record with the best signal-to-noise ratio and hand pick the onset of the phase; we then obtain the relative onset time of the phases on other records by the cross-correlation method. *SKKS* waveforms are Hilbert transformed before differential *SKKS-SKS* travel-time residuals are obtained by the cross-correlation method. Most of the cross-correlation values of different phases in our selected data are larger than 0.9, indicating little effect of attenuation or interference of other phases on the obtained travel times.

2.3. Travel-Time Corrections for the Effect of Seismic Heterogeneities Outside the Pacific Anomaly

[14] Two components of corrections for the effect of the seismic heterogeneities outside the Pacific Anomaly are considered. One component is the travel-time residuals predicted by the seismic heterogeneities outside the anomaly on the basis of Grand's model. The second component is additional travel-time variations owing to the underestima-

Table 1. Event List[a]

Number[b]	Event	Origin Time	Latitude (deg N)	Longitude (deg E)	Depth (km)	Time Correction (s)
	1998/01/26[c]	1998.01.26.23.06.01	−47.51 (−47.51)	165.19 (165.29)	33 (44)	5.0
	2000/11/07[d]	2000.11.07.07.50.09	−5.43 (−5.43)	154.02 (154.12)	91 (76)	0.5
	2002/04/24[d]	2002.04.24.11.00.00	−56.14 (−56.04)	−122.31 (−122.31)	10 (20)	3.5
1	2001/12/23	2001.12.23.22.52.54	−9.61 (−9.51)	159.53 (159.63)	16 (23)	5.0
2	1998/07/16	1998.07.16.11.56.36	−11.04 (−11.04)	166.16 (166.16)	110 (90)	−1.0
3	2000/01/09	2000.01.09.21.54.40	−18.82 (−18.78)	174.37 (174.62)	33 (30)	4.5
4	2001/05/26	2001.05.26.10.57.26	−20.29 (−20.19)	−177.84 (−177.54)	407 (407)	0.5
5	1997/09/04	1997.09.04.04.23.37	−26.47 (−26.42)	178.69 (178.59)	593 (592)	−1.0
6	1998/07/09	1998.07.09.14.45.39	−30.49 (−30.49)	−178.99 (−178.59)	130 (145)	3.0
7	1995/09/08	1995.09.08.01.15.28	−56.22 (−56.02)	−122.42 (−122.42)	10 (16)	3.0
	2003/10/15[e]	2003.10.15.02.19.44	−17.82 (−17.97)	−178.70 (−178.45)	583 (569)	0.0

[a]Values in parentheses are relocated latitude, longitude, and depth.
[b]Earthquakes used to constrain the structural features and velocity structure of the Pacific Anomaly. Events are represented by corresponding numbers in Figures 1, 3, 5, 6, 7, 8, 11, and 12.
[c]Earthquake used as reference event for the additional correction for the *SKS* data.
[d]Earthquakes used as reference events for the additional correction for the *SH* data.
[e]Earthquake used to discuss velocity structure and geometry of the northwestern boundary of the Pacific Anomaly.

tion of Grand's model. The correction of the first component is straightforward. We modify Grand's model by setting the velocity perturbation inside the Pacific Anomaly to be zero; we then calculate the travel-time perturbations along the raypaths associated with the actual event and station locations on the basis of the modified tomographic model. Because seismic stations are located in different tectonic provinces in Eurasia and southern South America, it is necessary to correct for underestimations on the basis of Grand's model.

[15] To calculate the underestimations of the tomographic model, we select events 2000/11/07, 2002/04/24 and 1998/01/26, whose *S* or *SKS* waves propagate outside the Pacific Anomaly, as reference events so that the additional corrections do not remove any contributions from the Pacific Anomaly. The additional correction at each station is the difference of the travel-time residual observed for the reference event and the prediction on the basis of Grand's model for the reference event. For both *S* and *SKS*, the predicted travel-time residuals on the basis of Grand's model exhibit similar patterns to those of the observed travel-time residuals across the stations, and can account for a large fraction of the observed travel-time delays (left and middle panels, Figure 2). We choose two events occurring in the Solomon Islands (2000/11/07) and the southern East Pacific Rise (2002/04/24) as reference events for corrections for the *S* waves recorded in the stations in Eurasia and southern South America (Figures 2a and 2d). After source relocation and correction on the basis of the tomographic model, most of the travel-time residuals for the reference events are smaller than 1.5 s (Figures 2c and 2f). Since some of the *SKS* waves in the selected data exit a high-velocity region in the CMB beneath Eurasia, we also select an event (1998/01/26) whose *SKS* phases propagate through the high-velocity region, but outside the Pacific Anomaly, to estimate the contribution of the high-velocity anomaly. This event occurs off the west coast of South Island, New Zealand, and is recorded in seismic stations in Eurasia (Figure 2g). The observed *SKS* travel-time residuals exhibit a complicated pattern from eastern Asia to mid-Eurasia that is well estimated on the basis of Grand's model (Figures 2g and 2h). Most underestimations of *SKS* travel-time residuals are smaller than 1 s (Figure 2i). These underestimations (Figures 2c, 2f, and 2i) are used as the second component of travel-time corrections for the effect of seismic heterogeneities outside the Pacific Anomaly.

3. Structural and Velocity Features of the Pacific Anomaly

[16] In this section, we first provide evidence for the existence of a structural gap that separates the Pacific Anomaly into two portions. We then present results of geometry and shear velocity structure of the two portions on the basis of waveform modeling and travel-time analysis. The data presented in this section have been corrected for the effects of earthquake mislocation and seismic heterogeneities outside the Pacific Anomaly, i.e., after procedures 1 and 2 outlined in section 2.2.

3.1. Structural Gap Between Two Portions

[17] The *SKS* travel-time residuals for four events 1997/09/04, 2001/05/26, 2000/01/09 and 2001/12/23, and the differential *SKKS-SKS* travel-time residuals for event 2001/05/26 clearly show the existence of a structural gap inside the Pacific Anomaly (Figure 1a). The seismic waves for the first 3 events sample the Pacific Anomaly in the northwest direction toward Eurasia, and the *SKS* waves for event 2001/12/23 sample the anomaly in the opposite direction toward southern South America. The *SKS* phases of event 1997/09/04 exhibit no travel-time delay between 88° and 98° and increasing travel-time delays from 1 s at 102° to 1.5 s at 115° (Figure 3a). The *SKS* phases for event 2001/05/26 show little travel-time delay between 86° and 120° (with the exception of one record having travel-time delays of −0.8 s within the error bars of no travel-time delay; see Figure 3b), while the differential *SKKS-SKS* travel times exhibit positive residuals from 4 s at 95° to 3 s at 115° (Figure 3b). The *SKS* travel-time residuals for event 2000/01/09 decrease from 1.8 s at 93° to 0 s at 113° (Figure 3c) and those for event 2001/12/23 scatter around ±2 s between 116° and 123° (Figure 3d). Note that no travel-time delays are observed for the *SKS* waves sampling a lower-mantle region beneath the Fiji Islands for all the events (Figure 1a). These observations are a robust feature and cannot be attributed to the mislocation of the earth-

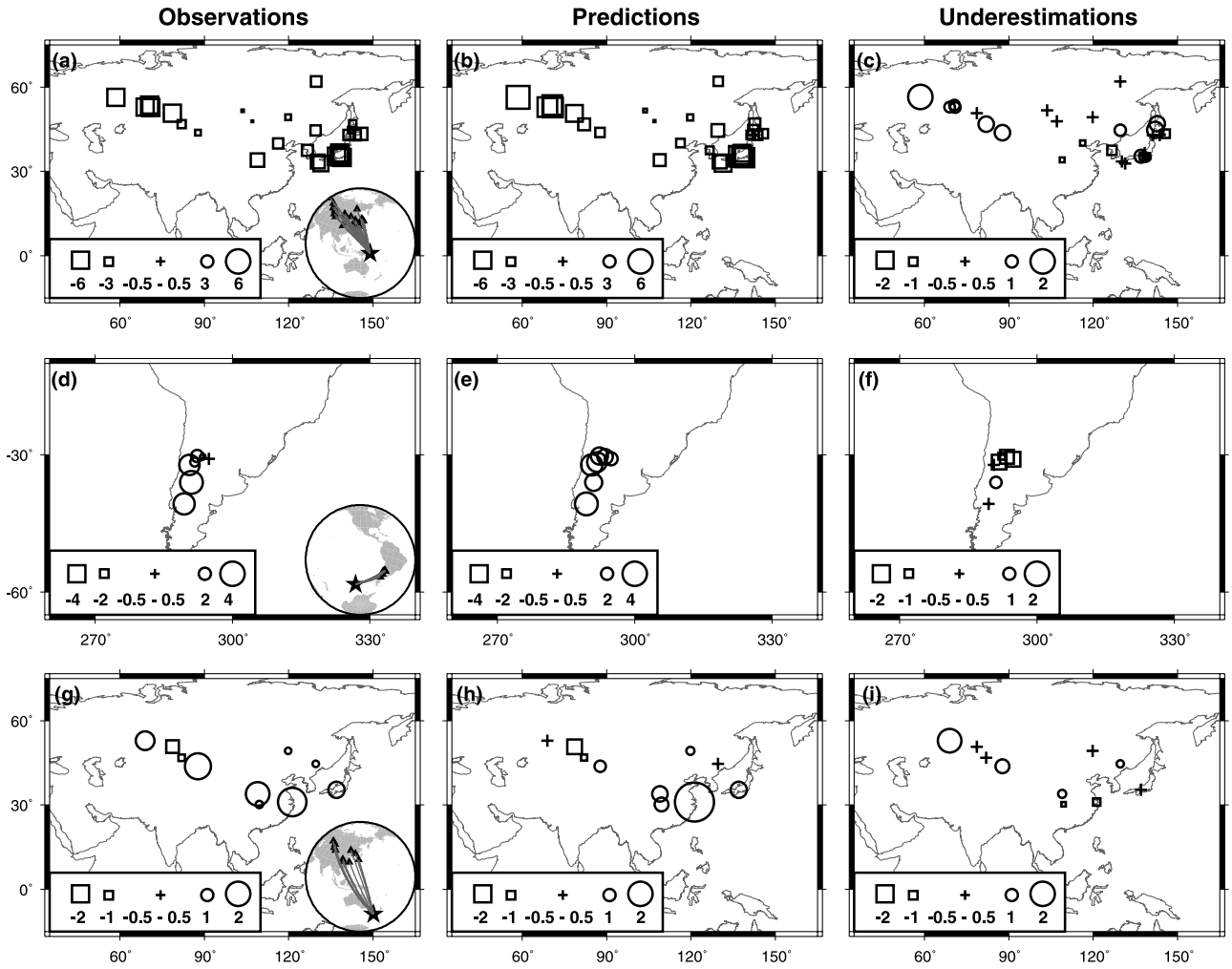

Figure 2. (a, d, and g) Observed direct *S* or *SKS* travel-time residuals for reference events, (b, e, and h) predicted *S* or *SKS* travel-time residuals for reference events on the basis of Grand's model, and (c, f, and i) observed *S* or *SKS* travel-time residuals for the reference events after corrected for the effects of the seismic heterogeneities outside the Pacific Anomaly on the basis of Grand's model. Note that the direct *S* or *SKS* phases for the reference events propagate outside the Pacific Anomaly. All these travel-time residuals are plotted with respect to the predictions on the basis of PREM and at the locations of each seismic station. The additional corrections in Figures 2c, 2f, and 2i are obtained by subtracting the travel-time residuals predicted on the basis of Grand's model (Figures 2b, 2e, and 2h) from those observed (Figures 2a, 2d, and 2g). Squares and circles denote positive and negative travel-time delays, respectively, with their sizes proportional to the magnitudes of travel-time delay. The great circle paths, event location of the reference event, and station locations are plotted in the bottom right corner of Figures 2a, 2d, and 2g.

quakes. First, these four events are relocated with very different data coverage, and, for all four events, the geographic locations of the entry points of these *SKS* phases without travel-time delays coincide with a same location in the lowermost mantle (Figures 3a–3d). Second, if we force the *SKS* phases of these events to have some travel-time delays and relocate these events, the root-mean squares of the differences between the observed direct *S* travel times and the calculated direct *S* travel times of those events become larger for all these events, and so do the differences for most of the stations (see examples in Figures 4a and 4b). In addition, such relocations yield uniform *SKS* travel-time residuals for the records at other stations in the similar azimuth. These relocation tests indicate that the observed no-travel-time delays of the *SKS* phases sampling the lower-mantle region beneath the Fiji Islands cannot be explained by changing earthquake locations.

[18] Note that *SKS* and *SKKS* phases of event 2001/05/26 exhibit different patterns of travel-time residuals (Figure 3b). Because these waves propagate along similar paths in the source-side upper mantle and receiver-side upper mantle and crust, they cannot be explained by seismic heterogeneities in the source and receiver-side upper mantle or crust. Note also that the observed travel-time residuals correlate with their entrant points in the source-side lower mantle (Figures 3a–3d), but not with the exit points in the receiver-

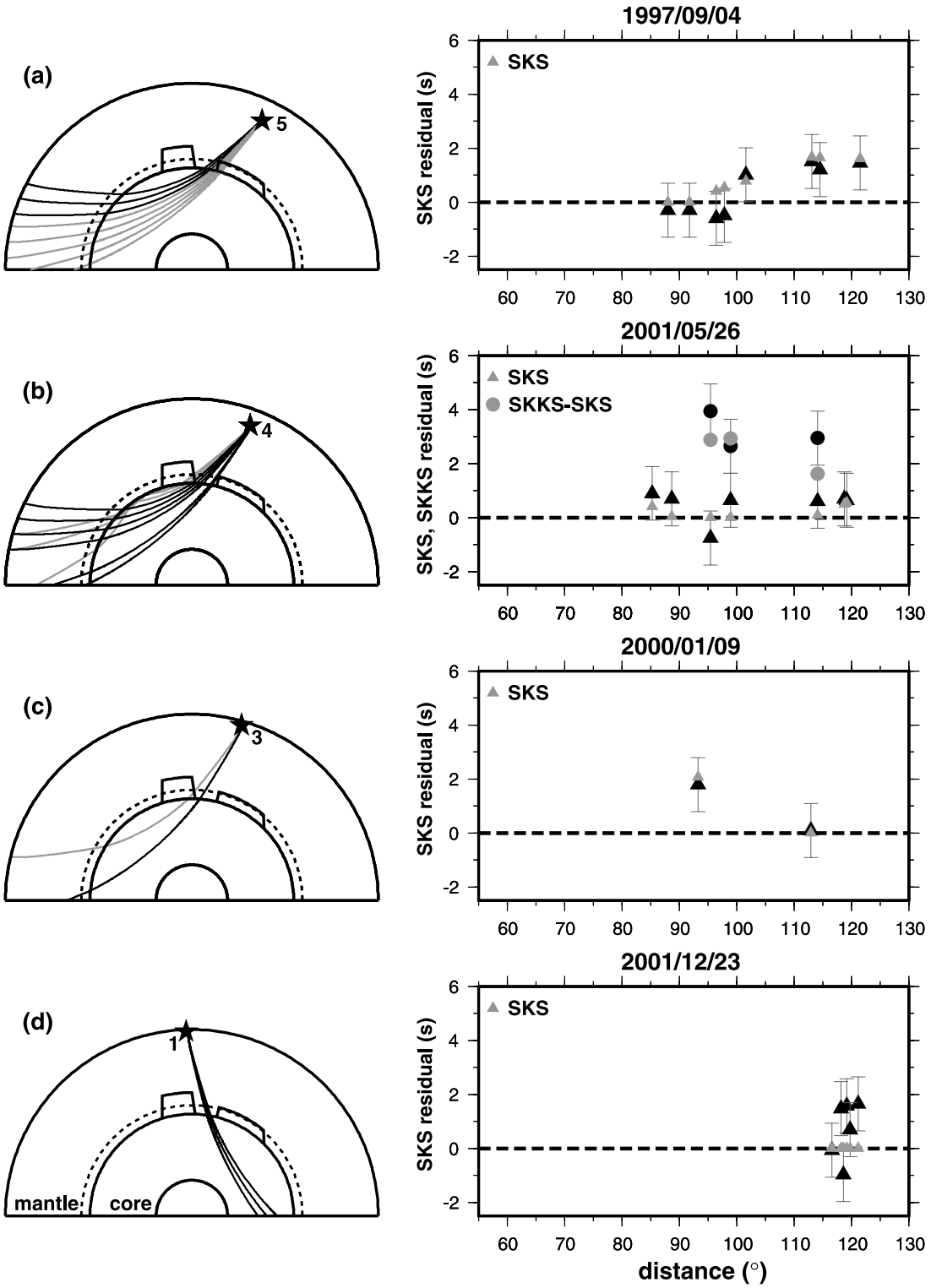

Figure 3. Left panels show *SKS* or *SKKS* raypaths with respect to the location of the best fitting model, with the paths of no-travel-time delays shown in a heavy color. The event numbers are the same as those in Figure 1. Right panels show observed *SKS* travel-time residuals (black triangles) or *SKKS-SKS* differential travel-time residuals (black circles) with respect to PREM as a function of epicentral distance and predictions (gray triangles or circles) on the basis of the best fitting model. The error bars in travel-time picks of 1 s are also shown.

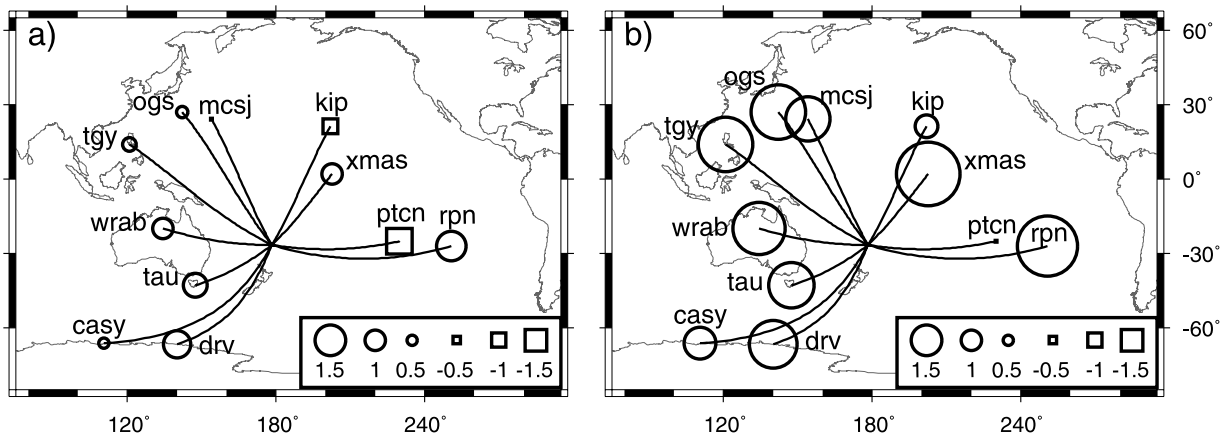

Figure 4. (a) Travel-time residuals of *SH* phases (black circles and squares) with respect to PREM predicted on the basis of the best fitting location of event 1997/09/04 and (b) a new location by forcing the travel-time residuals of *SKS* phase to be 2 s larger than shown in the original data. The effects of the seismic heterogeneities outside the Pacific Anomaly were corrected on the basis of Grand's model. Travel-time residuals are plotted at the locations of each station, along with the great circle path from event to stations.

side mantle. We show an example in Figures 3a and 3b, the *SKS* phases recorded for events 1997/09/04 and 2001/05/26 have similar propagation paths in the receiver-side mantle, but show different patterns of travel-time delay. The travel-time residuals observed for these events are thus not caused by the seismic structure beneath the receiver-side lower mantle. The no-travel-time delays of the *SKS* phases indicate a structural gap in the source-side lower mantle beneath the Fiji Islands within the Pacific Anomaly.

3.2. Structural and Velocity Features of the Western Portion of the Anomaly

[19] The direct *S*, *Sdiff*, *ScS* phases of events 1998/07/16, 1998/07/09, 2001/05/26 and 2000/01/09, the *SKS* phases of events 2000/01/09, 2001/12/23 and 1998/07/16, and the *SKKS* phases of event 2001/05/26 are used to constrain the geometry and velocity features of the western portion of the anomaly (Figures 1, 3, and 5). The direct *S*, *Sdiff* and *SKS* arrivals of event 1998/07/16 clearly identify the western boundary of the western portion of the anomaly. No travel-time delay is observed for the *S* and *Sdiff* phases of event 1998/07/16 between 60° and 120°, but travel-time delays of 3 s from 100° to 120° are observed for the *SKS* phases from the same event (see the right panel of Figure 5a). These observations indicate that the western boundary of the western portion of the anomaly is between the *SKS* and *SH* propagation paths of event 1998/07/16 (see the left panel of Figure 5a). The direct *S* travel-time residuals of events 1998/07/09 and 2001/05/26 are used to place constraints on the depth extent of the western portion of the anomaly (Figures 5b and 5c). The direct *S* phases of events 1998/07/09 and 2001/05/26 show no travel-time delay before 77°, suggesting the thickness of the western portion of the anomaly is about 740 km (Figures 5b and 5c). The eastern boundary of the western portion of the anomaly is constrained by *SKS* and *SKKS* arrivals from event 2001/05/26 (Figure 3b). Different from the *SKS* travel-time residuals, the travel-time delay of *SKKS* phases of event 2001/05/26 varies from 4.0 s at 95° to 3.0 s at 115° (Figure 3b). These observations indicate that the *SKKS* phases of event 2001/05/26 propagate inside the western portion of the anomaly, while the *SKS* phases at distances larger than 86° propagate outside it, placing constraints on the eastern boundary of the western portion of the anomaly. The *SKS* travel-time residuals for event 2000/01/09 decrease from 1.8 s at 93° to 0.0 s at 113°, and those for event 2001/12/23 scatter around ±2 s between 116° and 123°, providing constraints on the geometry and velocity structure of the eastern boundary of the western portion of the anomaly (Figures 3c and 3d).

[20] The above observations suggest that the western portion of the anomaly extends about 740 km above the CMB beneath the western Pacific with a 1050-km-wide base. With the thickness, and eastern and western boundaries of the western portion of the anomaly constrained, we test different geometries and velocity structures of the western portion of the anomaly on the basis of fitting the travel-time data. In additional to the *SKS* and *SKKS* travel-time residuals discussed above, the *S*, *Sdiff* and *ScS* travel-time residuals of events 1998/07/09, 2001/05/26 and 2000/01/09 are used to place further constraints on the structural feature and velocity structure of the western portion of the anomaly (see Figures 5b, 5c, and 5d, and the event locations in Figure 1). The direct *S* travel-time residuals of event 1998/07/09 increase rapidly with epicentral distance from 0 s at 78° to 5.6 s at 88°, and remain at about 4.5 s at distances between 90° and 108° (Figure 5b). The *S* travel-time delays of events 2001/05/26 and 2000/01/09 show similar patterns as those of event 1998/07/09 with maximum values of 5 s and 3 s, respectively (Figures 5c and 5d). Meanwhile, the *ScS* travel-time delays vary around 6.0 s from 75° to 79° for event 1998/07/09 (Figure 5b), decrease with increasing epicentral distance from 6.0 s at 70° to 5.0 s at 77° for event 2001/05/26 (Figure 5c), and decrease from 5.0 s at 65° to 3.0 s at 75° for event 2000/01/09 (Figure 5d). These observations are consistent with a trapezoidal-shape model (Figures 5a–5d).

[21] The *S* waves observed before 88° for event 1998/07/09 propagate a long distance inside the top part of the

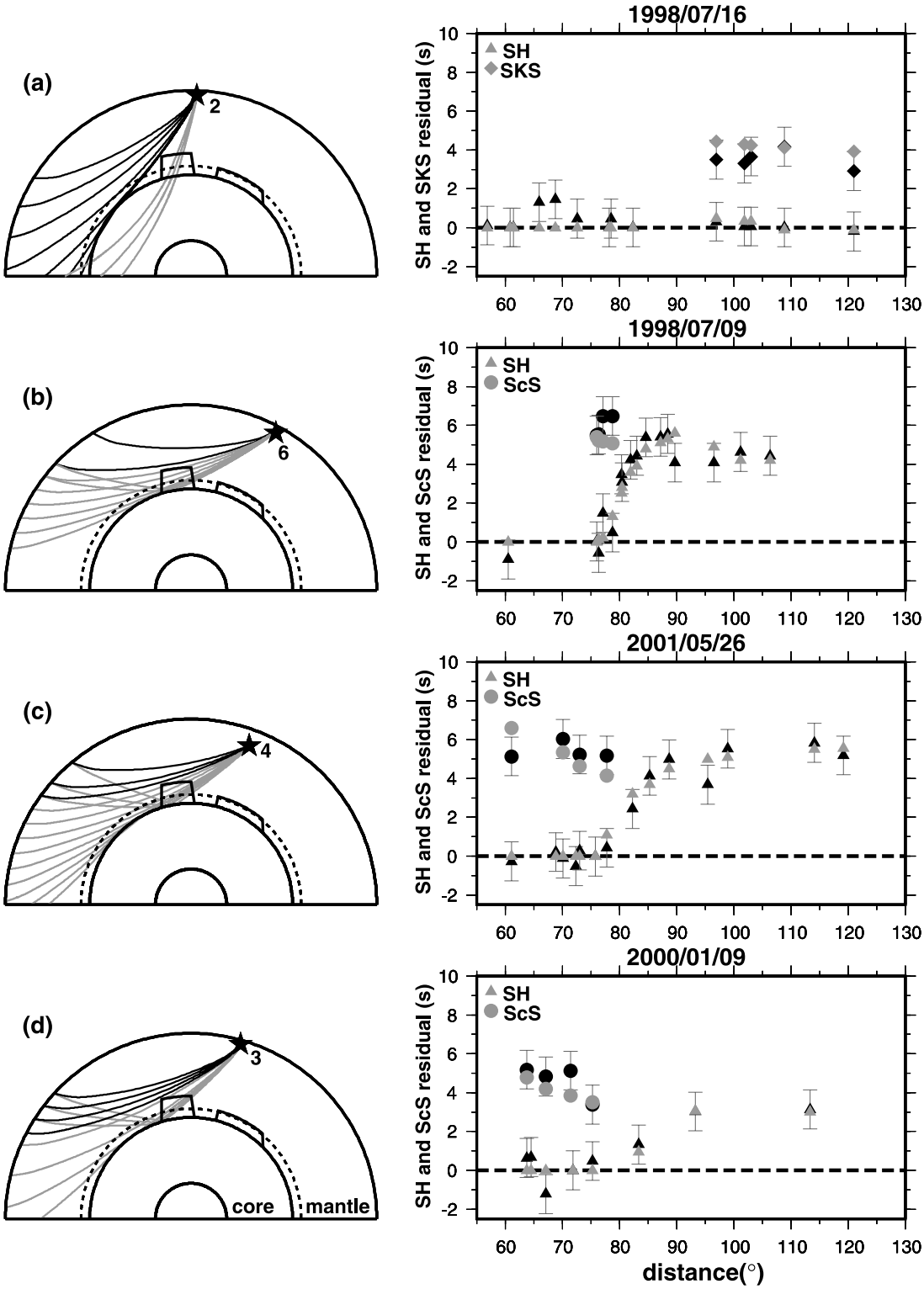

Figure 5. Left panels show *SH*, *ScS*, or *SKS* raypaths with respect to the location of the best fitting model, with the paths of no-travel-time delays shown with a heavy line. Events are numbered the same as in Figure 1. Right panels show observed *SH* travel-time residual (black triangle), *ScS* travel-time residual (black circle), or *SKS* (black diamond) travel-time residuals with respect to PREM and predictions (corresponding gray symbols) on the basis of the best fitting model. The error bars in travel-time picks of 1 s are also shown.

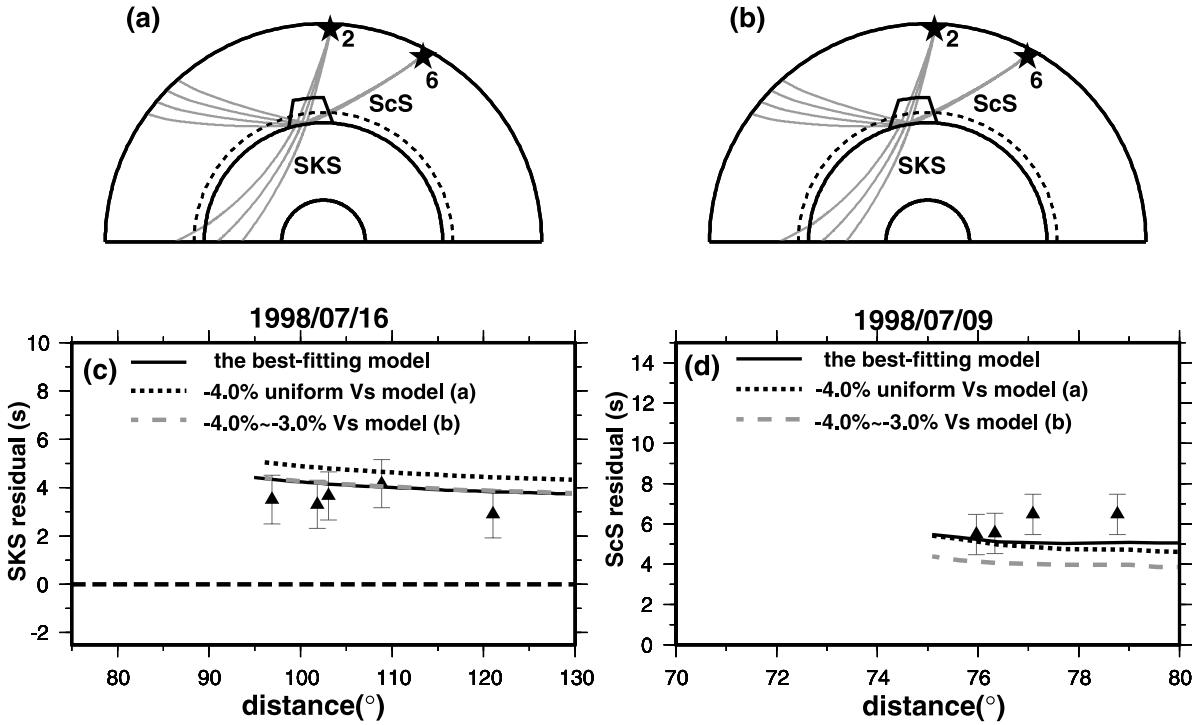

Figure 6. *SKS* raypaths of event 1998/07/16 (event 2 in Figure 1) and *ScS* raypaths of event 1998/07/09 (event 6 in Figure 1) with respect to the location of (a) a model with uniform velocity reduction of −4% and (b) another model with velocity reduction varying from −4.0% at the top to −3% at the bottom. The geometry of models shown in Figures 6a and 6b are constructed to be consistent with the observed abruptly increasing *SH* travel-time delays of event 1998/07/09. (c) Observed *SKS* travel-time residuals with respect to PREM for event 1998/07/16 (black triangles) and predictions for the best fitting model (black line) and models shown in Figures 6a and 6b (black and gray dashed lines, respectively). (d) Observed *ScS* travel-time residuals with respect to PREM for event 1998/07/09 (black triangles) and predictions for the best fitting model (black line) and models shown in Figures 6a and 6b (black and gray dashed lines, respectively).

western portion of the anomaly and exhibit anomalously large travel-time delays (Figure 5b). Those observations are sensitive to the geometry and velocity structure of the top part of the western portion of the anomaly. To match the abruptly increasing *S* travel-time delays of event 1998/07/09 between 78° and 88°, a velocity reduction of −3.0% and a width of 1000 km are needed in the top part of the western portion of the anomaly. There are some trade-offs between velocity structure and lateral extent of the anomaly. The absolute travel times calculated by a model with a wider (narrower) top part of the western portion of the anomaly and a smaller (larger) velocity reduction would also fit the observations well. However, a shear velocity reduction larger than −4.0% in the top portion of the anomaly would generate *SKS* travel-time delays larger than those observed for event 1998/07/16 (Figures 6a and 6c). Besides, if the velocity reduction is −4.0% in the top part of the western portion of the anomaly, a decrease of velocity reduction to −3.0% toward the CMB are needed to match the observed *SKS* travel-time delays of event 1998/07/16 (Figure 6b). In that case, the *ScS* travel-time delays calculated on the basis of such model would not fit the observations of event 1998/07/09 (Figure 6d). The *ScS* travel-time residuals would require the velocity reductions in the lowermost mantle to be larger than −4.0%. On the other hand, if the shear-velocity reduction is smaller than −2.0% in the top part of the western portion of the anomaly, a large increase of shear-velocity reduction with depth and a decrease in lateral dimension would be required to reproduce the large *SH* travel-time delays observed for event 1998/07/09 (Figures 7a and 7b). Such a model, however, would generate *ScS* travel-time delays between 55° and 65° larger than those observed for events 2001/05/16 and 1997/09/04 (Figures 7c and 7d), and therefore is unacceptable. The best fitting model for the western portion of the anomaly has a shear velocity reduction of about −3.0% in the top part of the anomaly. To explain all the data, the shear velocity reduction needs to increase from −3% in the top to −3.5% at the 100 km above the CMB and reach an average of −5% in the lowermost 100 km of the mantle.

[22] The best fitting model constrained by the above observations has a trapezoidal shape with its lateral dimension slightly increasing with depth. It extends 740 km above the CMB beneath the western Pacific and has a 1050-km-wide base extending both northwestward and southeastward. The model has a shear velocity structure with velocity reductions gradually increasing from −3.0% at 740 km above the CMB to −3.5% at the 100 km above the CMB, and an average velocity reduction of −5% in the base.

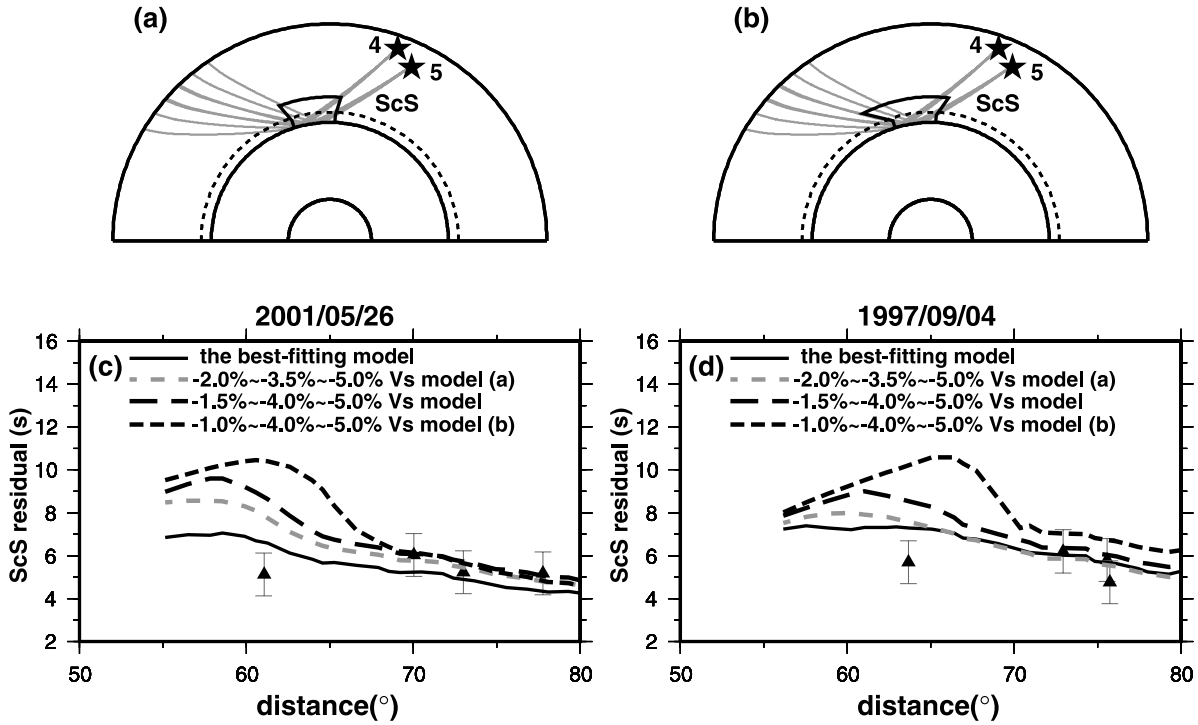

Figure 7. *ScS* raypaths of events 2001/05/26 (event 4 in Figure 1) and 1997/09/04 (event 5 in Figure 1) with respect to the locations of models are shown in Figures 7a and 7b. The model in Figure 7a has a shear-velocity structure of velocity gradually decreasing from −2.0% at 740 km above the CMB to −3.5% at the 100 km above the CMB, and velocity reductions of −5% in the base. The model shown in Figure 7b has a shear velocity structure of velocity gradually decreasing from −1.0% at 740 km above the CMB to −4.0% at the 100 km above the CMB, and velocity reductions of −5% in the base. The geometries of the models shown in Figures 7a and 7b are constructed to be consistent with the observed abruptly increasing *SH* travel-time delays of event 1998/07/09. Figures 7c and 7d show observed *ScS* travel-time residuals with respect to PREM for events 2001/05/26 and 1997/09/04 (black triangles) and predictions for the best fitting model (black line) and test models including those shown in Figures 7a and 7b (black and gray dashed lines).

3.3. Structure and Velocity Features of the Eastern Portion of the Anomaly

[23] The geometry and velocity features of the eastern portion of the anomaly are constrained by the travel times of direct *S* and *ScS* phases of events 1995/09/08 and 1997/09/04, *Sdiff* phase of event 1995/09/08, and *SKS* phase of event 1997/09/04 (Figures 1, 3, and 8). The direct *S* travel-time residuals of event 1995/09/08 place bounds on the depth extent of the eastern portion of the anomaly (Figure 8a). The direct *S* phases show no travel-time delay between 55° and 82°, indicating that the eastern portion of the anomaly extends to 650 km above the CMB. However, because of the absence of constraints from the *S* phases between 82° and 90°, the *S* wave travel-time delay of 3.0 s at 90° only confirms that the eastern portion extends more than 340 km above the CMB (Figure 8a). The western boundary of the eastern portion of the anomaly is constrained by the *SKS* phases of event 1997/09/04 recorded at the Eurasian stations (Figure 3a). The *SKS* phases of that event exhibit no travel-time delay at 88° and a gradual increase of delay to about 1 s at 92° and 1.5 s at 115° (Figure 3a). These observations can be explained by the model that the *SKS* wave recorded at the epicentral distance of 88° propagates outside the eastern portion of the anomaly and the *SKS* waves recorded at larger distances travel through the western boundary of the eastern portion of the anomaly. The eastern boundary of the eastern portion of the anomaly is constrained using the *S*, *ScS* and *SKS* phases of event 1997/09/04 recorded in stations in southern South America (Figure 8b). The *S* and *ScS* phases of event 1997/09/04 show no travel-time delay at 80°, and *SKS* phases exhibit travel-time delays of about 1.0–3.0 s between 82° and 105° (Figure 8b). These observations indicate that the eastern boundary of the eastern portion of the anomaly should locate between the propagation paths of the *ScS* and *SKS* phases of event 1997/09/04. The travel-time delays of *S* phases of event 1995/09/08 reach 9.0–11.2 s at the diffracted distances, and the *ScS* phases of event 1995/09/08 exhibit travel-time delays increasing from 2.0 to 3.0 s at 58° to 6.0 s at 76°, providing further constraints on the eastern boundary, geometry and velocity structure of the eastern portion of the anomaly (Figure 8a).

[24] Seismic data indicate that the eastern portion of the anomaly reaches at least 340 km above the CMB beneath the mid-Pacific and exhibits a trapezoidal shape with lateral dimension increasing slightly with depth. The base of the eastern portion of the anomaly is about 1800 km wide extending both northwestward and southeastward. A shear-

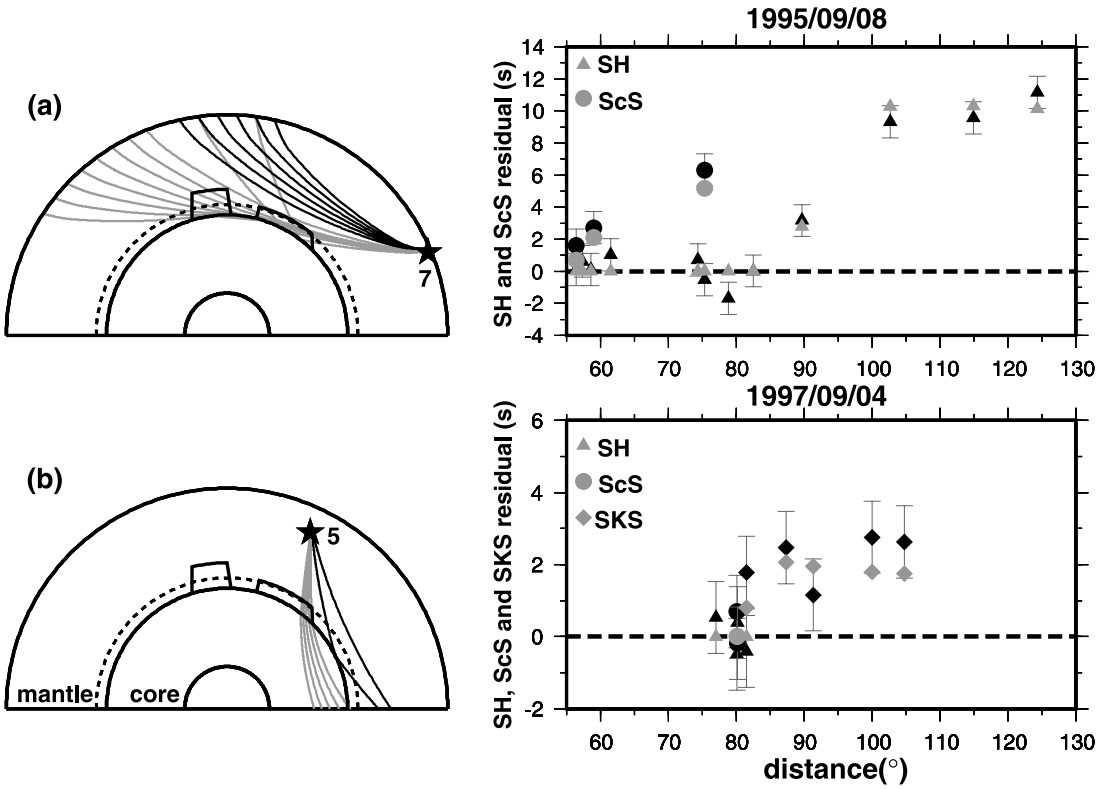

Figure 8. (a and b) Left panels show direct *SH*, *ScS*, and *SKS* raypaths of events 1995/09/08 (event 7 in Figure 1) and 1997/09/04 (event 5 in Figure 1) with respect to the location of the best fitting model. The paths of no-travel-time delays are shown with heavy lines. Right panels show observed *SH* travel-time residuals (black triangles), *ScS* travel-time residuals (black circles), and *SKS* travel-time residuals (black diamonds) with respect to PREM and predictions (corresponding gray symbols) on the basis of the best fitting model.

velocity structure with a uniform velocity reduction of −3% can fit the observations well. Because of the data sampling, the geometry and the velocity structure of the eastern portion of the anomaly are not well resolved.

3.4. General Structural Feature and Velocity Structure of the Pacific Anomaly

[25] Dense seismic data sampling has suggested that the detailed seismic structures within the Pacific Anomaly are more complex. Many localized ultralow-velocity zones (ULVZs) were detected near the CMB beneath the western Pacific region using anomalous *SKS-SPdKS* waveforms [e.g., *Garnero and Helmberger*, 1996; *Wen and Helmberger*, 1998a], *PKP* precursors [*Vidale and Hedlin*, 1998; *Wen and Helmberger*, 1998b], *ScP* precursors and postcursors [*Rost and Revenaugh*, 2003] and *ScS* travel times and waveforms [*He et al.*, 2006].

[26] The waveform data recorded in the NCISP and the CCSN for an earthquake 2003/10/15 occurring in the Tonga-Fiji subduction zone indicated existence of an ULVZ located near the edge of the western portion of the anomaly. The stations and source of this event are located along the great circle arc, and the *ScS* phases recorded for this event sample the northwestern boundary of the western portion of the anomaly (Figure 9a). In a previous study, we showed that the tangential displacements of event 2003/10/15 can be explained by a shear-velocity model with a velocity jump of about 2% at about 145 km above the CMB and a thin (30-km-thick) basal layer with a shear wave velocity reduction of −13% [*He et al.*, 2006], on the basis of one-dimensional modeling. Two dimensional (2-D) modeling, taking into consideration the geometry of the anomaly constrained along this great arc, suggests a similar feature, but the ULVZ could be localized just near the edge of the anomaly with a larger vertical scale of 100 km (Figure 9b). Such two-dimensional models could explain the seismic observations of event 2003/10/15 equally well (Figures 9c and 9d). The statement by *Takeuchi et al.* [2008] that our model was obtained under the assumption of the existence of an ultralow-velocity basal layer is incorrect. While the vertical scale of the ULVZ would depend on the overall 2-D structure adopted, an ULVZ is required to match the observed large amplitude of *SuS* phases (the *S* phase reflected off the top of the ULVZ) (Figure 9). The wave propagation through a complex three-dimensional structure may produce additional pulses in the seismograms through multipathing effects [*Helmberger and Ni*, 2005; *Ni et al.*, 2005]. In this case, we suggest that the observed large amplitudes of the *SuS* phases are likely caused by the 2-D effect, because the *SuS* phases have a similar moveout as that of the *ScS* phases more consistent with a reflection from the top of a thin layer above the CMB than from an off great circle path. The existence of the high-velocity layer adjacent to the Pacific Anomaly can also explain the observations

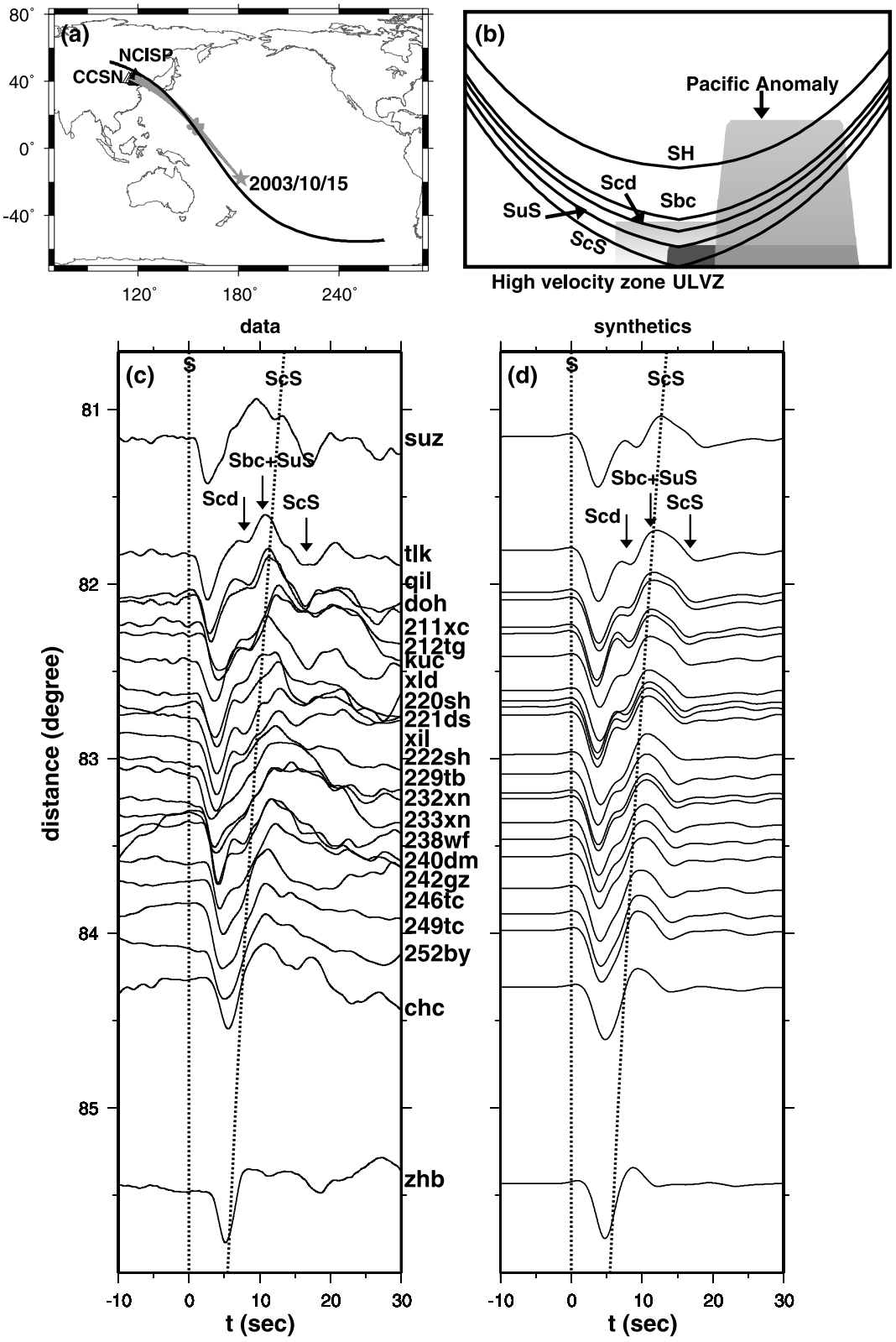

Figure 9. (a) Locations of event (gray star), seismic stations (triangles), and great circle paths (gray lines) of event 2003/10/15. The selected great circle arc is also shown by a bold line. (b) Schematic illustration of the raypaths of *SH*, *Sbc*, *Scd*, *SuS*, and *ScS* phases generated by the 2-D model. The arrivals of these phases are also labeled in the synthetics in Figure 9d. (c) Tangential displacements records for event 2003/10/15. The seismic waveforms are aligned along the calculated *SH* arrival on the basis of PREM. (d) Synthetics calculated on the basis of a 2-D model shown in Figure 9b.

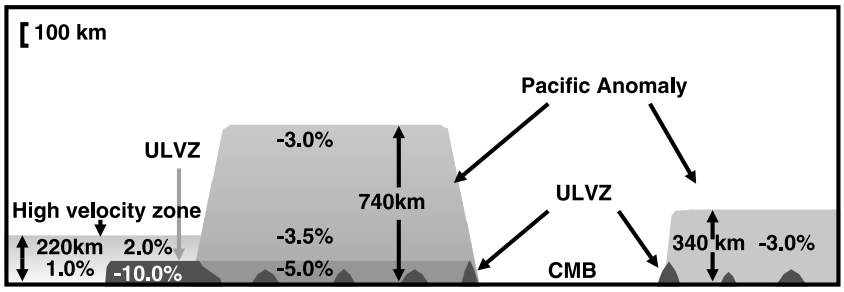

Figure 10. Inferred seismic structure across the Pacific Anomaly along the selected great circle arc from Eurasia to southern South America. The anomaly consists of two separated portions with a 740-km-wide gap between them. The western portion extends 740 km above the core-mantle boundary with a 1050-km-wide base. The eastern portion of the anomaly reaches at least 340 km above the core-mantle boundary and has an 1800-km-wide base. Ultralow-velocity zones (ULVZs) are located at the edge of the northwestern boundary of the western portion of the anomaly and at the base of the anomaly.

that the direct *S* travel-time residuals of event 1998/07/09 decrease from 5.6 s at 88° to about 4.5 s at distances between 90° and 108° (Figure 5b).

[27] The general structure of the Pacific Anomaly along the great arc from eastern Eurasia to southern South America is schematically illustrated in Figure 10. The Pacific Anomaly consists of two large separated portions extending into the middle-lower mantle and small-scale ULVZs situated at its base and edge. There is a 740-km-wide gap between two major portions. The western portion of the anomaly extends about 740 km above the CMB beneath western Pacific and exhibits a trapezoidal shape with a 1050-km-wide base. The eastern portion of the anomaly reaches at least 340 km above the CMB beneath the mid-Pacific and exhibits a trapezoidal shape with lateral dimensions increasing slightly with depth. The base of the eastern portion of the anomaly is about 1800 km wide extending both northwestward and southeastward. The western portion of the anomaly has a shear velocity structure with velocity reductions from −3.0% at the top to −3.5% at 100 km above the CMB, and to −5.0% in the bottom 100 km of the mantle. The eastern portion of the anomaly has a uniform velocity reduction of −3.0%. At the base of the mantle, the Pacific Anomaly is surrounded by a high-velocity region in northwest with a velocity jump of about 2% at 220 km above the CMB. An ULVZ with a thickness of 100 km and a shear velocity reduction of −10% extends beneath the high-velocity layer.

4. Discussion

[28] In this section, we examine various geometries and shear-velocity structures of the Pacific Anomaly and discuss implications of the inferred geometry and seismic structure of the anomaly. As not many constraints on the shape of the eastern portion of the anomaly exist, we focus our discussions only on the western portion of the anomaly.

4.1. A Model With Bell-Like Geometry

[29] A bell-like geometry is found for the African Anomaly in the lower mantle, with both flanks tilting toward its center and the width increasing with depth [*Wang and Wen*, 2007]. As we discussed above, the shear-velocity reduction in the top part of the anomaly should be between −2.0% and −4.0% in order to fit the magnitude of the abruptly increasing *SH* travel-time delays of event 1998/09/07 and the *SKS* travel-time residuals of event 1998/07/16. For this magnitude of velocity reduction, the width of the top part of the western portion of the Pacific Anomaly should be larger than 750 km (Figure 11). This minimal width of the top of

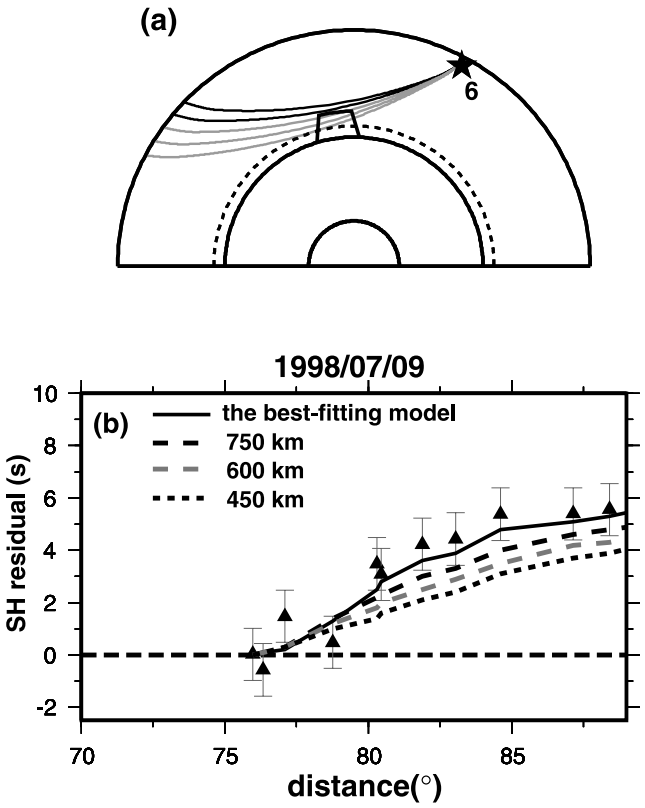

Figure 11. (a) Direct *S* raypaths of event 1998/07/09 (event 6; see Figure 1a) with respect to the location of a trapezoid-shaped model. The velocity structure varies from −3.5% at the top to −5% at the base of the mantle. The paths of no-travel-time delays are shown with thicker lines. (b) Observed direct *SH* travel-time residuals with respect to PREM for event 1998/07/09 (black triangles) and predictions for the best fitting model (black line) and trapezoid-shaped models with various widths in the top part of the anomaly (dashed lines; labeled with the widths).

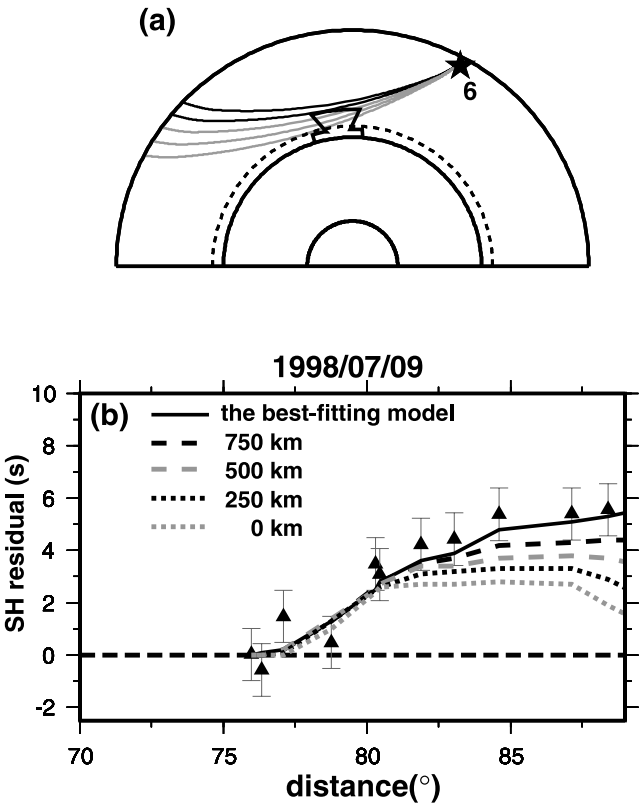

Figure 12. (a) Direct *SH* raypaths of event 1998/07/09 (event 6; see Figure 1a) with respect to the location of plume-like models. The models have a wide head of 1000 km, a narrow tail, and a widened base layer with the same extent in the best fitting model. The paths of no-travel-time delays are shown with heavy lines. (b) Observed direct *SH* travel-time residuals with respect to PREM for event 1998/07/09 (black triangles) and predictions calculated on the basis of the best fitting model (bold line) and plume-like models with various widths for the tail (dashed lines; labeled with the widths).

the anomaly is only slightly smaller than the lateral extent of the base (1050 km), indicating the flanks of the western portion of the anomaly are steeper than those of the African Anomaly.

4.2. A Model With Mushroom-Like Geometry

[30] A mushroom-like geometry may result from a buoyant, thermal or thermochemical mantle plume, erupting from the CMB [e.g., *Richards et al.*, 1989; *Davaille et al.*, 2003]. Here we test a series of plume-like models, consisting of a wide head, a narrow tail and a wide basal layer (Figure 12a). As the velocity structure and the lateral extents of the top and bottom of the anomaly are independently constrained by the seismic data discussed above, we set the velocity structure and the top and bottom lateral extents of the anomaly as those in the best fitting model. We test models with the width of the narrowest part of models varying from 750 to 0 km. Synthetics calculated on the basis of these models show a decrease or slight increase of *SH* travel-time delays with increasing distance after 82° when width of the tail is smaller than 750 km, while the observations show that the *SH* travel-time delays increase from 0 s at 78° to 5.6 s at 88° (Figure 12b). Our observations indicate that, if the western portion of the anomaly has a mushroom-like geometry, its tail width cannot be smaller than 750 km.

4.3. Implications of the Inferred Geometry and Seismic Structure

[31] The trapezoidal shape with a wide top and steep flanks of the Pacific Anomaly is consistent with the geometry inferred for a metastable thermochemical pile in the study of *Tan and Gurnis* [2005]. Both the geographic gap and geometry of the western portion of the Pacific Anomaly indicate that the Pacific Anomaly is less stable compared to the African Anomaly, possibly owing to slight differences in composition and/or enrichment of heat-producing elements between the two anomalies. The presence of ULVZs at the base and edge of the Pacific Anomaly further indicates existence of vigorous small-scale convection at the base of the Pacific Anomaly. Partial melt is likely required to explain the large velocity reductions inferred for these ULVZs. The geographic locations of these ULVZs support the hypothesis that these ULVZs may represent similar chemical heterogeneities like the African and Pacific anomalies, but in different length scales with different degrees of melt [*Wen et al.*, 2001]. Because the current seismic data prevent us from resolving a velocity structure between an average shear-velocity reduction of −5% and a strong negative shear-velocity gradient in the bottom 100 km of the Pacific Anomaly, it is also possible that partial melt in the Pacific Anomaly may extend a few hundred kilometers above the CMB as it does at the base of the African Anomaly [*Wen et al.*, 2001].

5. Conclusion

[32] We determine structural and shear-velocity features of the Pacific Anomaly on the basis of forward travel-time analysis and waveform modeling of direct *S*, *Sdiff*, *ScS*, *SKS* and *SKKS* phases sampling a great arc across the anomaly from eastern Eurasia to southern South America. The seismic data suggest that the Pacific Anomaly consists of two large separated portions extending into the middle-lower mantle and small-scale ULVZs situated at its base and edge. There is a 740-km-wide gap between the two major portions. The western portion of the anomaly extends 740 km above the CMB beneath the western Pacific and exhibits a trapezoidal shape with a 1050-km-wide base. The eastern portion of the anomaly reaches at least 340 km above the CMB beneath the mid-Pacific and exhibits a trapezoidal shape with an 1800-km-wide base. The shear velocity structure of the western portion has velocity reductions of −3.0% at the top increasing to −3.5% at 100 km above the CMB, and an average velocity reduction of −5.0% in the bottom 100 km of the mantle. The eastern portion has an average shear-velocity reduction of −3.0%. At the base of the mantle, waveform modeling further suggests the Pacific Anomaly is surrounded by a high-velocity region in northwest with a velocity jump of about 2% at 220 km above the CMB and an ULVZ with shear velocity reduction of −10% extends beneath the high-velocity layer. The geographic gap, geometry and velocity structure of the Pacific Anomaly

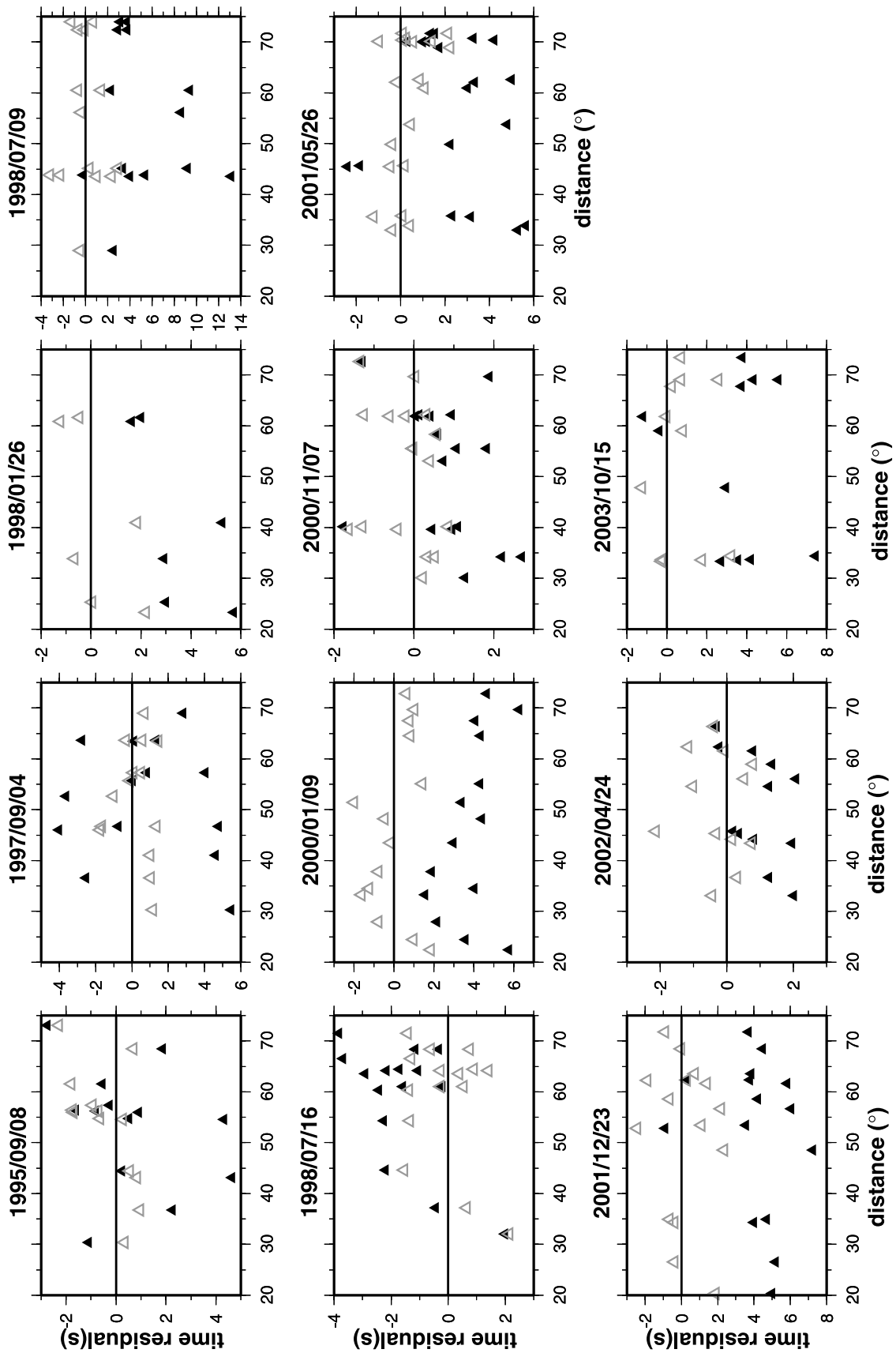

Figure A1. *SH* travel-time residuals with respect to PREM before (black triangles) and after (open triangles) source relocations. The effect of the seismic heterogeneities outside the Pacific Anomaly was removed on the basis of Grand's tomographic model.

suggest that the Pacific Anomaly represents a cluster of metastable thermochemical piles. The presence of ULVZs at the base and edge of the anomaly indicates existence of vigorous small-scale convection and partial melt at the base of the anomaly.

Appendix A: Earthquake Relocation

[33] We hand-picked the onset of the arrival times of direct *S* and *sS* phases recorded by the Global Seismographic Network (GSN) between 20° and 75° to relocate all the earthquakes used in this study (see Table 1 and Figure A1). We have excluded the *S* and *sS* phases recorded at distances larger than 75°, because they could sample, and be affected by, the Pacific Anomaly in the lower mantle. The relocation process consists of two steps.

[34] 1. Within a 4° × 4° × 20 km × 10 s space-time range (longitude, latitude, focal depth and time) centered at the original event longitude, latitude, focal depth and origin time presented in the Incorporated Research Institution for Seismology (IRIS), we carry out a grid search with an interval of 0.5° in longitude, 0.5° in latitude, 2 km in focal depth and 1 s in origin time for the best fitting location and origin time. The best fitting location and origin time is the one that predicts the smallest root-mean square of the differences between the observed direct *S* and *sS* travel times and the calculated direct *S* and *sS* travel times on the basis of the assumed new location and origin time and a global shear velocity tomographic model (S. Grand, personal communication, 2004).

[35] 2. Repeat the process, using the new longitude, latitude, focal depth and origin time as the original earthquake parameters and perform the search within a 1° × 1° × 4 km × 7 s space-time range with a grid with intervals of 0.1° in longitude, 0.1° in latitude, 1 km in focal depth and 0.5 s in origin time. Relocation results are presented in Table 1. The relocation significantly reduces the travel-time misfits for the GSN observations (Figure A1).

[36] **Acknowledgments.** We gratefully acknowledge the participants of the CNDSN, the Incorporated Research Institutions for Seismology, and the F-net for their efforts in collecting the data. We thank Sean Ford and Michael Wysession for their helpful comments, which improved this article. Figures were made with the General Mapping Tools [*Wessel and Smith*, 1995]. This work was supported by the National Science Foundation of China (grants 40774041 and 40434012) and NSF grant 0609717.

References

Avants, M., T. Lay, and E. J. Garnero (2006), A new probe of ULVZ S-wave velocity structure: Array stacking of *ScS* waveforms, *Geophys. Res. Lett.*, *33*, L07314, doi:10.1029/2005GL024989.

Bréger, L., and B. Romanowicz (1998), Three-dimensional structure at the base of the mantle beneath the central Pacific, *Science*, *282*, 718–720, doi:10.1126/science.282.5389.718.

Davaille, A., M. Le Bars, and C. Carbonne (2003), Thermal convection in a heterogeneous mantle, *C. R. Geosci.*, *335*, 141–156, doi:10.1016/S1631-0713(03)00003-8.

Dziewonski, A. M. (1984), Mapping the lower mantle: Determination of lateral heterogeneity in P-velocity up to degree and order-6, *J. Geophys. Res.*, *89*, 5929–5942, doi:10.1029/JB089iB07p05929.

Ford, S. R., E. J. Garnero, and A. K. McNamara (2006), A strong lateral shear velocity gradient and anisotropy heterogeneity in the lowermost mantle beneath the southern Pacific, *J. Geophys. Res.*, *111*, B03306, doi:10.1029/2004JB003574.

Garnero, E. J., and D. V. Helmberger (1996), Seismic detection of a thin laterally varying boundary layer at the base of the mantle beneath the central Pacific, *Geophys. Res. Lett.*, *23*, 977–980, doi:10.1029/95GL03603.

Grand, S. P. (2002), Mantle shear-wave tomography and the fate of subducted slabs, *Philos. Trans. R. Soc. London, Ser. A*, *360*, 2475–2491, doi:10.1098/rsta.2002.1077.

Gu, Y. J., A. M. Dziewonski, W. J. Su, and G. Ekström (2001), Models of the mantle shear velocity and discontinuities in the pattern of lateral heterogeneities, *J. Geophys. Res.*, *106*, 11,169–11,199, doi:10.1029/2001JB000340.

He, Y., L. Wen, and T. Zheng (2006), Geographic boundary and shear wave velocity structure of the Pacific anomaly near the core mantle boundary beneath the western Pacific, *Earth Planet. Sci. Lett.*, *244*, 302–314, doi:10.1016/j.epsl.2006.02.007.

Helmberger, D. V., and S. Ni (2005), Approximate 3D body-wave synthetics for tomographic models, *Bull. Seismol. Soc. Am.*, *95*, 212–224, doi:10.1785/0120040004.

Ishii, M., and J. Tromp (1999), Normal-mode and free-air gravity constraints on lateral variations in velocity and density of the Earth's mantle, *Science*, *285*, 1231–1236, doi:10.1126/science.285.5431.1231.

Kustowski, B., G. Ekström, and A. M. Dziewoñski (2008), Anisotropic shear-wave velocity structure of the Earth's mantle: A global model, *J. Geophys. Res.*, *113*, B06306, doi:10.1029/2007JB005169.

Lay, T., J. Hernlund, E. J. Garnero, and M. S. Thorne (2006), A post-perovskite lens and D″ heat flux beneath the central Pacific, *Science*, *314*, 1272–1276, doi:10.1126/science.1133280.

Li, X., and B. Romanowicz (1996), Global mantle shear velocity model developed using nonlinear asymptotic coupling theory, *J. Geophys. Res.*, *101*, 22,245–22,272, doi:10.1029/96JB01306.

Masters, G., S. Johnson, G. Laske, and H. Bolton (1996), A shear-velocity model of the mantle, *Philos. Trans. R. Soc. Ser. A.*, *354*, 1385–1410, doi:10.1098/rsta.1996.0054.

Masters, G., G. Laske, H. Bolton, and A. M. Dziewonski (2000), The relative behavior of shear velocity, bulk sound speed, and compressional velocity in the mantle: Implications for chemical and thermal structure, in *Earth's Deep Interior: Mineral Physics and Tomography From the Atomic to the Global Scale*, *Geophys. Monogr. Ser.*, vol. 117, edited by S. Karato et al., pp. 63–87, AGU, Washington, D.C.

Mori, J., and D. V. Helmberger (1995), Localized boundary layer below the mid-Pacific velocity anomaly identified from a PcP precursor, *J. Geophys. Res.*, *100*, 20,359–20,365, doi:10.1029/95JB02243.

Ni, S., and D. V. Helmberger (2003), Seismological constraints on the South African superplume; could be the oldest distinct structure on Earth, *Earth Planet. Sci. Lett.*, *206*, 119–131, doi:10.1016/S0012-821X(02)01072-5.

Ni, S., D. V. Helmberger, and J. Tromp (2005), Three-dimensional structure of the African superplume from waveform modeling, *Geophys. J. Int.*, *161*, 283–294, doi:10.1111/j.1365-246X.2005.02508.x.

Ohta, K., K. Hirose, T. Lay, N. Sata, and Y. Ohishi (2008), Phase transitions in pyrolite and MORB at lowermost mantle conditions: Implications for a MORB-rich pile above the core-mantle boundary, *Earth Planet. Sci. Lett.*, *267*, 107–117.

Richards, M. A., R. A. Duncan, and V. E. Courtillot (1989), Flood basalts and hot-spot tracks: Plume heads and tails, *Science*, *246*, 103–107, doi:10.1126/science.246.4926.103.

Ritsema, J., S. Ni, and D. V. Helmberger (1998), Evidence for strong shear velocity reductions and velocity gradients in the lower mantle beneath Africa, *Geophys. Res. Lett.*, *25*, 4245–4248, doi:10.1029/1998GL900127.

Ritsema, J., H. Jan Van Heijst, and J. H. Woodhouse (1999), Complex shear wave velocity structure imaged beneath Africa and Iceland, *Science*, *286*, 1925–1928, doi:10.1126/science.286.5446.1925.

Rost, S., and J. Revenaugh (2003), Small-scale ultralow-velocity zone structure imaged by *ScP*, *J. Geophys. Res.*, *108*(B1), 2056, doi:10.1029/2001JB001627.

Russell, S. A., C. Reasoner, T. Lay, and J. Revenaugh (2001), Coexisting shear- and compressional-wave seismic velocity discontinuities beneath the central Pacific, *Geophys. Res. Lett.*, *28*, 2281–2284, doi:10.1029/2000GL012553.

Su, W. J., R. L. Woodword, and A. M. Dziewonski (1994), Degree 12 model of shear velocity heterogeneity in the mantle, *J. Geophys. Res.*, *99*, 6945–6980, doi:10.1029/93JB03408.

Takeuchi, N., Y. Morita, N. D. Xuyen, and N. Q. Zung (2008), Extent of the low-velocity region in the lowermost mantle beneath the western Pacific detected by the Vietnamese Broadband Seismograph Array, *Geophys. Res. Lett.*, *35*, L05307, doi:10.1029/2008GL033197.

Tan, E., and M. Gurnis (2005), Metastable superplumes and mantle compressibility, *Geophys. Res. Lett.*, *32*, L20307, doi:10.1029/2005GL024190.

To, A., B. Romanowicz, Y. Capdeville, and N. Takeuchi (2005), 3D effects of sharp boundaries at the borders of the African and Pacific superplumes: Observations and modeling, *Earth Planet. Sci. Lett.*, *233*, 137–153, doi:10.1016/j.epsl.2005.01.037.

Van der Hilst, R. D., and H. Kárason (1999), Compositional heterogeneity in the bottom 1000 kilometers of Earth's mantle: Toward a hybrid convection model, *Science*, *283*, 1885–1888, doi:10.1126/science.283.5409.1885.

Vidale, J. E., and M. A. Hedlin (1998), Evidence for partial melt at the core-mantle boundary north of Tonga from the strong scattering of seismic waves, *Nature*, *391*, 682–685, doi:10.1038/35601.

Wang, Y., and L. Wen (2004), Mapping the geometry and geographic distribution of a very low velocity province at the base of the Earth's mantle, *J. Geophys. Res.*, *109*, B10305, doi:10.1029/2003JB002674.

Wang, Y., and L. Wen (2007), Geometry and P and *S* velocity structure of the "African Anomaly," *J. Geophys. Res.*, *112*, B05313, doi:10.1029/2006JB004483.

Wen, L. (2001), Seismic evidence for a rapidly varying compositional anomaly at the base of the Earth's mantle beneath the Indian Ocean, *Earth Planet. Sci. Lett.*, *194*, 83–95, doi:10.1016/S0012-821X(01)00550-7.

Wen, L. (2002), An *SH* hybrid method and shear velocity structures in the lowermost mantle beneath the central Pacific and South Atlantic Oceans, *J. Geophys. Res.*, *107*(B3), 2055, doi:10.1029/2001JB000499.

Wen, L. (2006), A compositional anomaly at the Earth's core-mantle boundary as an anchor to the relatively slowly moving surface hotspots and as source to the DUPAL anomaly, *Earth Planet. Sci. Lett.*, *246*, 138–148, doi:10.1016/j.epsl.2006.04.024.

Wen, L., and D. V. Helmberger (1998a), A two-dimensional P-SV hybrid method and its application to localized structures near the core-mantle boundary, *J. Geophys. Res.*, *103*, 17,901–17,918, doi:10.1029/98JB01276.

Wen, L., and D. V. Helmberger (1998b), Ultra-low velocity zones near the core-mantle boundary from broadband *PKP* precursors, *Science*, *279*, 1701–1703, doi:10.1126/science.279.5357.1701.

Wen, L., P. Silver, D. James, and R. Kuehnel (2001), Seismic evidence for a thermo-chemical boundary at the base of the Earth's mantle, *Earth Planet. Sci. Lett.*, *189*, 141–153, doi:10.1016/S0012-821X(01)00365-X.

Wessel, P., and W. H. F. Smith (1995), New version of the Generic Mapping Tools released, *Eos Trans. AGU*, *76*(33), 329.

Y. He, Key Laboratory of the Earth's Deep Interior, Institute of Geology and Geophysics, Chinese Academy of Sciences, Beijing 100029, China. (ymhe@mail.igcas.ac.cn)

L. Wen, Department of Geosciences, State University of New York at Stony Brook, Stony Brook, NY 11794, USA.